The current issue and full text archive of this journal is available on Emerald Insight at:
https://www.emerald.com/insight/1573-6105.htm

Evaluation method of equivalent initial flaw size and fatigue life prediction of nickel-based single crystal superalloy

Zhixun Wen, Fei Li and Ming Li
School of Mechanics Civil Engineering and Architecture, Northwestern Polytechnical University, Xi'an, China and State Key Laboratory of Clean and Efficient Turbomachinery Power Equipment, Xi'an, China

Received 10 August 2023
Revised 5 September 2023
Accepted 11 September 2023

Abstract

Purpose – The purpose of this paper is to apply the concept of equivalent initial flaw size (EIFS) to the anisotropic nickel-based single crystal (SX) material, and to predict the fatigue life on this basis. The crack propagation law of SX material at different temperatures and the weak correlation of EIFS values verification under different loading conditions are also investigated.

Design/methodology/approach – A three-parameter time to crack initial (TTCI) method with multiple reference crack lengths under different loading conditions is established, which include the TTCI backstepping method and EIFS fitting method. Subsequently, the optimized EIFS distribution is obtained based on the random crack propagation rate and maximum likelihood estimation of median fatigue life. Then, an effective driving force based on anisotropic and mixed crack propagation mode is proposed to describe the crack propagation rate in the small crack stage. Finally, the fatigue life of three different temperature ESE(T) standard specimens is predicted based on the EIFS values under different survival rates.

Findings – The optimized EIFS distribution based on EIFS fitting - maximum likelihood estimation (MLE) method has the highest accuracy in predicting the total fatigue life, with the range of EIFS values being about [0.0028, 0.0875] (mm), and the mean value of EIFS being 0.0506 mm. The error between the predicted fatigue life based on the crack propagation rate and EIFS distribution for survival rates ranges from 5% to 95% and the experimental life is within two times dispersion band.

Originality/value – This paper systematically proposes a new anisotropic material EIFS prediction method, establishing a framework for predicting the fatigue life of SX material at different temperatures using fracture mechanics to avoid inaccurate anisotropic constitutive models and fatigue damage accumulation theory.

Keywords Equivalent initial flaw size, Nickel-based single crystal superalloy, Fatigue life prediction, Crack growth rate, ESE(T) specimen

Paper type Research paper

Nomenclature

a	crack length, mm	$a(0)_{5/95}$	the value of 5% probability of transcending number and 95% confidencelevel, mm
a_{IFS}	initial crack length, mm	C, m	Paris formula fitting coefficient
a_{ave}	average initial crack length, mm	Cov	noise value
a_b	detectable crack length, mm	D_i	the data set D between the cycle number of the ith observation N_i and
a_c	critical crack length, mm		
a_r	reference crack length, mm		

The research was supported by the National Natural Science Foundation of China (52105147), National Science and Technology Major Project (J2019-IV-0011–0079), and Innovation Foundation for Doctor Dissertation of Northwestern Polytechnical University (No. CX2021068).

Multidiscipline Modeling in Materials and Structures
Vol. 19 No. 6, 2023
pp. 1311-1338
© Emerald Publishing Limited
1573-6105
DOI 10.1108/MMMS-08-2023-0256

	the crack length a_i seen through experiments
E	error factors
$f_a(x), f_a(a\|t)$	probability density function of the initial crack length
$F(v, a_i)$	the formula for calculating fatigue life
$F(a/W)$	geometric correction factor for stress intensity factor
$g(\mu, \sigma^2, v)$	EIFS probability density function
$g_{update}(\mu, \sigma^2, v)$	update EIFS probability density function
H	undetermined coefficient in crack length expression
$K_{\max}$	maximum stress intensity factor, MPa$\sqrt{\text{m}}$
$K_{\text{I}}, K_{\text{II}}, K_{\text{III}}$	three stress intensity factors, MPa$\sqrt{\text{m}}$
K_{IC}	fracture toughness of type I crack, MPa$\sqrt{\text{m}}$
K_{eff}	effective stress intensity factor, MPa$\sqrt{\text{m}}$
$\overline{m}_{\text{EIFS}}$	the mean value of EIFS probability density function
N	number of cycles (or fatigue life)
N_i	number of cycles under the upper and lower limits of the integral are the v_i and a_c, respectively
N_m	the median number of cycles
Q, b	fitting coefficient between the crack length growth rate ($\text{d}a/\text{d}t$) and the crack length
Q_i	fitting coefficient for type ith stress level (or condition)
$P(D)$	the probability of detected crack length
V	equivalent variable of EIFS value
$\widetilde{V}$	equivalent variable of EIFS value with error
X	random crack propagation parameter
x_u	upper limit for EIFSD
$Y(\rho)$	anisotropy correction factor
$\sigma_{\max}$	maximum stress, MPa
σ^2, μ	variance and mean of variable V
(α, β, γ)	TTCI or EIFS distribution function parameters
$\exists$	total number of test samples
ω	measurement error caused by temperature

1. Introduction

The nickel-based single crystal superalloys (SX) are remarkable for their resistance to mechanical and chemical degradation at temperatures up to 1000 °C and beyond, which find application in a range of jet engines and land-based turbines. As a crucial component of engines, the research on material properties, the study of material properties and strength life of single crystal turbine blades is very important. In terms of simple fatigue loads, extensive research has been conducted on material failure mechanisms, deformation mechanisms and life models construction etc. (Nazé *et al.*, 2022; Le Graverend *et al.*, 2014; Wang *et al.*, 2023), but the analysis results are often far from the test data and lack repeatability. The reason is that the fatigue life is controlled by three coupling factors of material, environment and manufacture, and it is very complicated to describe it accurately.

At present, a lot of research has been conducted on the mechanism of the influence of microstructure on strength of SX materials. During the *in situ* tension process, microcracks often generate between the carbide and the matrix, and the carbide itself also cracks to accelerate the propagation of the main crack (Ma *et al.*, 2010). In the process of high temperature creep, microcracks usually occur at the interface between the TCP phase and the γ matrix phase or in the stress concentrated interaction region (Liu *et al.*, 2017; Tan *et al.*, 2013; Tian *et al.*, 2014). Compared with tensile and creep conditions, fatigue crack initiation and

propagation are more complicated. The discontinuous or non-uniform microstructure (such as porosity, carbide or eutectic) on the surface or subsurface of single crystal materials can easily induce irreversible cyclic dislocation slip during cyclic loading, resulting in local plastic strain accumulation and crack initiation (Cervellon *et al.*, 2020). The specific cracking location mainly depends on the applied stress, temperature, frequency, as well as the size, shape and position of the defect (Ormastroni *et al.*, 2020; Cervellon *et al.*, 2017, 2018; Lamm and Singer, 2007; Jiang *et al.*, 2018). In general, crack initiation occurs in the largest pores in the alloy (Ormastroni *et al.*, 2020; Cervellon *et al.*, 2018; Lamm and Singer, 2007; Jiang *et al.*, 2018). In addition, the decrease of the distance between the pore and the surface or the increase of pore irregularity will also promote the initiation of cracks (Lamm and Singer, 2007; Jiang *et al.*, 2018). When the pores in the alloy are eliminated by hot isostatic pressing, fatigue cracks may also be generated at the carbide (Cervellon *et al.*, 2018; Yi *et al.*, 2007), which was observed by Lu *et al.* (2013) and (Cervellon *et al.*, 2017) through *in situ* tensile at high temperature and low-cycle fatigue response. For longer duration tests (with low stress or frequency), the oxide layer may be the main crack initiation site (Cervellon *et al.*, 2018; Rémy *et al.*, 2013). Similarly, the initial defects can significantly affect the very-high cycle fatigue (VHCF) behavior of SX materials (Cervellon *et al.*, 2018, 2020). In general, there are defects in microstructure of monocrystalline materials and crystal anisotropy of the materials, resulting in more errors in the damage accumulation description model. It cannot be ignored that cracks or crack-type defects may occur during the processing of mechanical structures, and these damages will gradually form cracks during the test.

The definition of crack initiation in structural components is currently uncertain. Some scholars suggested that the crack initiation length should be 0.1 mm, but in most cases, when microcracks reach this scale, it will steadily propagate along the material cross-section (Claude *et al.*, 2013). The boundary between crack initiation and propagation is not clear, and there is no precise description method for the life of the initiation stage. Therefore, fracture mechanics often encounters bottlenecks in predicting the full fatigue life. The concept of equivalent initial flaw size (EIFS) is introduced to quantify the initial defects caused by materials, structures and manufacturing processes. As a starting point for life calculation, the whole fatigue life of a structure is only expressed as the crack growth stage (Rice and Broek, 1978). The EIFS theory was first proposed by Yang and Manning (1980), Rudd and Gray (1976), and then Wang (1982) applied it to the structural durability analysis, considering that the initial damage of the structure cannot be directly measured and assuming it as an imaginary crack (a_0). Various methods for predicting fatigue life derived from this method have been adopted by many researchers, such as Correia *et al.* (2016), who completed EIFS calculations based on double plate fatigue tests and obtained the maximum total fatigue life from the approximate initial defect size. According to a comparative study conducted by Al-Mukhtar *et al.* (2010), the inverse theory was optimized, and the calculated accuracy of the probabilistic total fatigue life obtained seems to be acceptable. Liang *et al.* (2019) and Liu and Mahadevan (2009) proposed a method for determining EIFS based on the Kitagawa-Takahashi diagram to avoid the dependence of equivalent crack size on stress level. Statistical methods such as maximum likelihood estimation (MLE) (Zhuang *et al.*, 2023; Makeev *et al.*, 2007) or Bayesian update (Torregosa and Hu, 2013; Morse, 2020) take into account the source of uncertainty in the backward inference process, and obtain the probability description of EIFS to effectively improve the prediction accuracy.

The crack propagation behavior of SX materials is significantly different from that of common metals. Previous studies (Sakaguchi *et al.*, 2019; Reed, 2008) have reported that crack initiation and propagation are closely related to crystal orientation, load and temperature, and depend on the strength of the strengthening phase (γ' phase) and matrix phase (γ phase). Traditional linear elastic fracture mechanics (LEFM) cannot simply determine the driving force of crack growth based on the stress intensity determined by ΔK, although the crack

growth life can be combined with Paris' law to establish the crack growth rate based on ΔK (Zhang *et al.*, 2019; Musinski and McDowell, 2012; Paris, 1963). These models are often described in terms of damage parameters such as maximum plastic strain and maximum decomposing shear stress (Zhang *et al.*, 2019; Hong *et al.*, 2011). In addition, SX materials exhibit different fracture modes at different temperatures and crystal direction, usually type I fracture perpendicular to the loading axis and mixed crack propagation along the crystal surface (Li *et al.*, 2023), which further increases the difficulty of description.

To sum up, the application of EIFS mainly focuses on isotropic materials, and the inferred EIFS values are closely related to the structure and experimental environment. Therefore, this article applies the principle of probabilistic fracture mechanics to derive the EIFS theory and establishes a new universal EIFS distribution (EIFSD) that can describe the initial fatigue quality of the structure to reduce the dependence of the experimental environment. The rationality of EIFS theory is verified through SX material fatigue crack propagation experiments, and the fatigue life is predicted using fracture mechanics to avoid inaccurate anisotropic constitutive models and fatigue damage accumulation theory. This method can quantitatively evaluate the initial damage state of the material, provide a reference for guiding the manufacture of single crystal blades and provide a new idea for further analyzing the fatigue life of stress concentrated parts of blades.

2. Theoretical formulation

2.1 Initial flaw size

After the actual structure is manufactured, there are often defects, inclusions, micropores, notches, steps and other materials or geometric discontinuities. Suppose that the probability of a crack with equivalent crack size a being detected in a single inspection is denoted as $P(D|a)$. To derive the distribution of $P(a)$ from $P(D|a)$, it can be assumed that the probability density function of the original crack length in the component is $f_a(x)$, where x is the existing crack length, then

$$P(x) = f_a(x)\mathrm{d}x \tag{1}$$

Therefore, the probability that a defect of size x exists and is detected is $P(D|a)\cdot f_a(x)\cdot \mathrm{d}x$, and the probability that crack lengths of various sizes in the structure are detected is:

$$P(D) = \int_0^\infty P(D|a)\cdot f_a(x)\cdot \mathrm{d}x \tag{2}$$

where $f_D(x)$ represents the probability density function of the detected crack size, and $P(x|D)$ represents the probability of detecting the crack length x. According to Bayes' formula:

$$P(x|D) = \frac{P(D|x)P(x)}{P(D)} = \frac{P(D|x)f_a(x)\mathrm{d}x}{\int_0^\infty P(D|a)\cdot f_a(x)\cdot \mathrm{d}x} \tag{3}$$

If $P(x|D)$ is approximated as $f_D(x)\mathrm{d}x$, then there is

$$f_D(x) = \frac{P(D|x)f_a(x)}{\int_0^\infty P(D|a)\cdot f_a(x)\cdot \mathrm{d}x} \tag{4}$$

In the above equation, $P(D|x)$ can be fitted using Weibull distribution (Wang *et al.*, 1996), and $f_D(x)$ is obtained from non-destructive testing analysis. Therefore, the probability density function of the initial length is:

$$f_a(x) = \frac{f_D(x)}{P(D|x)} \int_0^{\infty} P(D|x) \cdot f_a(x) \cdot \mathrm{d}x \tag{5}$$

Furthermore, crack length values that meet different confidence levels and survival rates can be determined based on $f_a(x)$, such as the average initial crack length a_{ave} and the average fatigue life N_{ave}, which can be expressed as Eq. (6). Based on experience, initial crack distribution law, crack propagation rate and experimental fatigue life, $f_a(x)$ is iteratively obtained.

$$\begin{cases} N_{ave} = \int_{a_{ave}}^{a_c} \dfrac{\mathrm{d}N}{\mathrm{d}a} \mathrm{d}a \\ a_{ave} = \int_{-\infty}^{+\infty} x f_a(x) \mathrm{d}x \end{cases} \tag{6}$$

2.2 EIFS probability distribution

Considering that the artificial determination of crack length during non-destructive testing cannot comprehensively consider the original state of materials and structures, the EIFSD is used instead. This method equivalently represents the entire life of the structure as crack propagation life, as shown in Figure 1. The damage before the small crack is regarded as EIFS, and the fatigue life prediction is carried out in combination with the crack growth rate at the small crack stage. The function expression is as follows:

$$\begin{aligned} N = S_I + S_{III} &= \int_{a_{IFS}}^{a_c} \left(\frac{1}{\mathrm{d}a/\mathrm{d}N} \right)_{\text{Ture}} \mathrm{d}a = \int_{a_{IFS}}^{a_b} \left(\frac{1}{\mathrm{d}a/\mathrm{d}N} \right)_{I} \mathrm{d}a + \int_{a_b}^{a_c} \left(\frac{1}{\mathrm{d}a/\mathrm{d}N} \right)_{III} \mathrm{d}a \\ &= \int_{EIFS}^{a_c} \left(\frac{1}{\mathrm{d}a/\mathrm{d}N} \right)_{II+III} \mathrm{d}a = S_{II} + S_{III} \end{aligned} \tag{7}$$

It is often very difficult to obtain the EIFSD by obtaining $P(D|x)$ according to Section 2.1, which is computationally complex and requires a prior distribution. The time to crack initial detectable reference crack length is defined as the TTCI, and the entire reverse inference process is shown in Figure 2. Within the range of approximate small cracks, the crack growth function expression used by Gallaher in the study of small cracks in aircraft structures (Gallagher and Molent, 2015), where Q and b are constants.

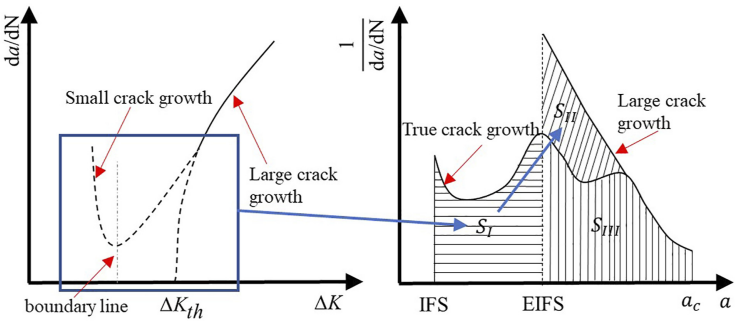

Source(s): Authors own work

Figure 1.
Fatigue life predicted by EIFS method

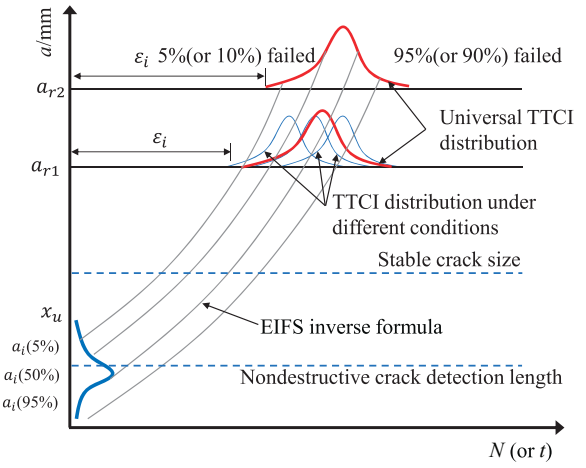

Source(s): Authors own work

Figure 2. Schematic representation of TTCI theory in order to obtain the EIFSD

$$\frac{\mathrm{d}a(t)}{\mathrm{d}t} = C\left(\Delta\sigma \cdot c_1 \cdot a(t)^{b1}\right)^m = Qa(t)^b \tag{8}$$

The solution of Q_i under a stress level often requires multiple fractures (k) to achieve fracture inversion, and each fracture has a Q_k value. Assuming there are m $(\mathrm{d}a/\mathrm{d}t, a)$ data points on a fracture surface, that is, obtaining a set of $(\mathrm{d}a/\mathrm{d}t, a)$ or (t, a) data requires a specific crack length a_j (time t_j) and its fatigue band spacing of the specimen. By fitting, it can be obtained:

$$Q_k = \frac{m\sum_{j=1}^{m} t_j \ln a_j - \sum_{j=1}^{m} \ln a_j \sum_{j=1}^{m} t_j}{m\sum_{j=1}^{m} t_j^2 - \left(\sum_{j=1}^{m} t_j\right)^2} = \exp\left[\left(m\sum_{j=1}^{m} \ln\left(\frac{\mathrm{d}a(t)}{\mathrm{d}t}\right)_j - \sum_{j=1}^{m} \ln a_j\right) \Big/ m\right] \tag{9}$$

Fit all fracture observation points under the same stress to obtain $Q_1, Q_2 \ldots Q_k$ and $b_1, b_2 \ldots b_k$ respectively, specify several crack lengths $(a_1, a_2 \ldots a_q)$ to be fitted and interpolate the fitting curves at these lengths to obtain data points,. (t_1, a_1), $(t_2, a_2) \ldots (t_q, a_q)$ and then obtain Q_i according to Eq. (9).

Perform indefinite integration on Eq. (8), and when $b_i > 1$, the relationship between crack size and time can be obtained as:

$$a(t) = [(1 - b_i)(Q_i t + H)]^{\frac{1}{1-b_i}} \tag{10}$$

Assuming that at time t_0, $a(t_0) = a_r$ (a_r is the reference crack length), then the undetermined coefficient $H = \frac{a_r{}^{(1-b_i)}}{1-b_i} - Qt_0$. Therefore, when $t = 0$,

$$EIFS = a(0) = \left[a_r{}^{(1-b_i)} - Q_i a_r (1 - b_i)\right]^{\frac{1}{1-b_i}} \tag{11}$$

Set the upper limit for EIFSD to x_u, and according to the above equation, the lower bound of the TTCI distribution (TTCID) can be obtained as:

$$\varepsilon_i = \frac{1}{(b_i - 1)Q_i}\left[{x_u}^{-(1-b_i)} - {a_r}^{-(1-b_i)}\right], \quad a_r \geq x_u \tag{12}$$

Specifying b_i as a fixed constant (such as $b_i = 1$) will simplify the problem, and of course, Q_i will also change, but it will try to fit Eq. (8) to the fracture data as much as possible. Therefore, at this point b_i and Q_i are no longer "material constants", but rather artificially specified constants for the convenience of EIFS solution. Based on this assumption, Eqs. (10) - (12) can be written as:

$$\begin{cases} EIFS = a_r \exp(-Q_i t) \\ \varepsilon_i = \dfrac{1}{Q_i}\left(\dfrac{a_r}{x_u}\right) \end{cases} \tag{13}$$

Assuming that TTCID follows the Weibull distribution and EIFS is treated as a random variable x, from a statistical perspective, the EIFSD and TTCID are compatible. The probability density and cumulative probability distribution functions of EIFS can be obtained as shown in Eq. (14), where α_i,β_i and ε_i are the shape parameter, scale parameter and lower bound of the TTCID function under the i-th stress, respectively.

$$\begin{cases} f_x(x) = \dfrac{\alpha_i}{\beta_i x}\left(\dfrac{\ln(x_u/x)}{Q_i\beta_i}\right)^{\alpha_i - 1} \exp\left[-\left(\dfrac{\ln(x_u/x)}{Q_i\beta_i}\right)^{\alpha_i}\right], \quad 0 < x < x_u \\ F_x(x) = \exp\left[-\left(\dfrac{\ln(x_u/x)}{Q_i\beta_i}\right)^{\alpha_i}\right], \quad 0 < x < x_u \end{cases} \tag{14}$$

(1) TTCI backstepping method

To determine α_i,β_i and ε_i and crack propagation parameters (Q_i and β_i), assuming that under a given reference crack length, the time corresponding to the e-th fracture among all k fractures is t_e, are arranged in ascending order as $t_1 < t_2 < \ldots < t_e < \ldots < t_k$, and the average rank estimation of the cumulative probability distribution corresponding to is:

$$F_T(t_e) = \frac{r}{k+1} \tag{15}$$

Among them, r is the t_e rearranged position, and k is still the total number of fractures under the i-th stress. The parameter $Q\beta$ in the EIFSD under the same reference crack are considered as the mean of $Q_i\beta_i$ in each stress level (Eq. (16)) to eliminate the effects of temperature, and further nominal crack propagation parameters at any stress level can be obtained.

$$\begin{cases} Q\beta = \dfrac{1}{L}\sum_{i=1}^{L} Q_i\beta_i \\ \widehat{Q} = Q\beta/\beta_i \end{cases} \tag{16}$$

In order to determine the parameter α, considering the dimension of the cumulative TTCID as 1, and the random variable W is constructed:

$$W = \widehat{Q}t_e - \ln\left(\frac{a_r}{x_u}\right) \tag{17}$$

And Eq. (14) can be rewritten as:

$$F_W(w) = 1 - \exp\left[-\left(\frac{w - \ln(a_r/x_u)}{Q\beta}\right)^{\alpha_i}\right] \tag{18}$$

In this case, $F_W(w)$ satisfies the two-parameter Weibull distribution of α_i and $Q\beta$. Although α_i and $Q\beta$ are independent of stress, in order to improve the reliability of backstepping results, all fracture data are collected, with a total of $n = L \cdot k$ values for W. Arrange W in ascending order to obtain the average rank estimate of the cumulative distribution probability corresponding to $F_W(w_l)$ as follows:

$$F_W(w_l) = \frac{l}{n+1}, \quad l = 1, 2, ..., n \tag{19}$$

Taking the quadratic logarithm on both sides of Eq. (18) can be simplified to the least squares form ($Z = \alpha X + B$). Changing (a_r, x_u) will result in different $(\alpha, Q\beta)$, and in order to obtain the best $(x_u, \alpha, Q\beta)$, the sum of squares (SSE) of the deviations between the theoretical and experimental values of the cumulative distribution function and the corresponding statistical values at each stress level is minimized. Substitute w_l into the theoretical value of $F_W(w_l)$ calculated by Eq. (18), and use Eq. (19) to calculate its experimental value $F_W{}'(w_l)$, then

$$\min SSE = \sum_{l=1}^{N} [F_W(w_l) - F_W{}'(w_l)]^2$$

$$s.t. \begin{cases} Z = \ln\{-\ln[1 - F_T(t)]\} \\ X = \ln W = \ln\left[\widehat{Q}t_e - \ln\left(\frac{a_r}{x_u}\right)\right] \\ B = -\alpha \ln Q\beta \\ \alpha = \dfrac{\sum Z}{\sum X - N \ln(Q\beta)} \end{cases} \tag{20}$$

(2) EIFS fitting method

Under the specified (or optimal) reference crack length a_r, all specimen values x_{ie} of each i-th stress (or other variable) level constitute the EIFS variable sample. From Eq. (14), it can be seen that the EIFS distribution follows a three parameter Weibull compatible distribution. This equation is transformed twice by natural logarithms ($Z = \alpha Y + b$), and

$$\begin{cases} Z = \ln\{-\ln F_X(x)\} \\ Y = \ln\ln(x_u/x) \\ b = -\alpha \ln Q\beta \end{cases} \tag{21}$$

Arrange x_m in ascending order, with Z being the corresponding ordinal number. The $F_X(x_m)$ corresponding to x_m can be estimated from the average rank distribution.

$$Q\beta = \exp(-b/\alpha) \tag{22}$$

Changing (a_r, x_u) to obtain different $(\alpha, Q\beta)$, in order to obtain the best $(x_u, \alpha, Q\beta)$, there are:

$$\min SSE = \sum_{m=1}^{N} \left\{ \frac{m}{N+1} - \exp\left[-\left(\frac{\ln(x_u/x_m)}{Q\beta} \right)^{\alpha} \right] \right\}^2 \tag{23}$$

2.3 Random crack propagation probability and EIFSD updating

2.3.1 Description of random crack growth rate. From the above description, it can be concluded that the power exponential expression of crack propagation rate concentrates on the dispersion of the fitted data on the Q value after a fixed index b. Therefore, Eq. (8) can be further rewritten as:

$$Q = \frac{\mathrm{d}a(t)/\mathrm{d}t}{a(t)^b} \tag{24}$$

Undimensionalise $a(t)$ and take the logarithm:

$$\frac{\mathrm{d}a(t)}{\mathrm{d}t} = Q\left(\frac{a(t)}{V}\right)^b \Rightarrow \ln\frac{\mathrm{d}a(t)}{\mathrm{d}t} = \ln Q + b\ln a(t) - b\ln V \tag{25}$$

There are many parameters to be considered in the three-parameter Weibull distribution. In order to achieve roughly the same accuracy and reduce parameter estimation, the EIFS value changing over time is further transformed into a lognormal distribution to facilitate the derivation of the safety crack length under different failure rates. Moreover, the lognormal distribution can predict the lower average failure rate faster than the two-parameter Weibull distribution (Tuegel *et al.*, 2018). Assuming $\ln V$ follows a normal distribution (V follows a normal distribution), its mean μ and variance σ^2, that is $\ln V \sim N(\mu, \sigma^2)$. If $a = \ln Q$, $x_i = \ln a(t)$ and $y_i = \ln[\mathrm{d}a(t)/\mathrm{d}t]$, the above equation can be rewritten as:

$$y_i = a - b\mu + bx_i - N\left(0, b^2\sigma^2\right) \tag{26}$$

Thus, y_i follows a normal distribution $y_i \sim N(a - b\mu + bx_i, b^2\sigma^2)$, and its probability density function is:

$$f\left(y_i, a, b, \mu, \sigma^2\right) = \frac{1}{\sqrt{2\pi}b\sigma}\exp\left[-\frac{(y_i - a + b\mu - bx_i)^2}{2b^2\sigma^2} \right] \tag{27}$$

If $\mu = 0$, the MLE method is used to estimate unknown parameters a, b and σ (Pieracci, 1995):

$$\begin{cases} b^2\sigma^2 = \dfrac{\sum_{i=1}^{n}(y_i - a - bx_i)^2}{n} \\ a = \dfrac{1}{n}\sum_{i=1}^{n} y_i - \dfrac{b}{n}\sum_{i=1}^{n} x_i \end{cases} \tag{28}$$

$$\frac{\mathrm{d}a(t)}{\mathrm{d}t} = \exp[\ln Q + b\ln a(t) - b\ln V] = Qa(t)^b \cdot \exp\left[N\left(0, b^2\sigma^2\right)\right] \tag{29}$$

Since $\exp[N(0, b^2\sigma^2)]$ follows the lognormal distribution, assuming parameters $X = \exp[N(0, b^2\sigma^2)]$ and $q(a) = Qa(t)^b$, the above equations can be randomized to $\mathrm{d}a(t)/\mathrm{d}t = q(a)\cdot X$, and integrated it to obtain:

$$\int_{a_0}^{a} \frac{1}{q(v)} \mathrm{d}v = \int_{t_0}^{t} X \mathrm{d}t = X(t - t_0) \tag{30}$$

When $t_0 = 0$, the parameter X and its differentiation over a can be written as Eqs (31) - (32).

$$X = \frac{1}{t} \int_{a_0}^{a} \frac{1}{Qa(t)^b} \mathrm{d}v = \frac{{a_0}^{1-b} - a^{1-b}}{tQ(b-1)} \tag{31}$$

$$\frac{\mathrm{d}X}{\mathrm{d}a} = \frac{a^{-b}}{tQ} \tag{32}$$

The probability density function of crack length a can be expressed as:

$$\begin{aligned} f_a(a) &= f_X\left(\frac{{a_0}^{1-b} - a^{1-b}}{tQ(b-1)}\right) \cdot \frac{1}{tQa(t)^b} \\ &= \frac{1}{\sqrt{2\pi}\sigma_X \cdot \dfrac{{a_0}^{1-b} - a^{1-b}}{tQ(b-1)}} \cdot \frac{\mathrm{d}X}{\mathrm{d}a} \cdot \exp\left\{ -\frac{1}{2}\left[-\frac{\ln\left(\frac{{a_0}^{1-b} - a^{1-b}}{(b-1)}\right) - \ln(tQ)}{\sigma_X} \right]^2 \right\} \\ &= \frac{a^{-b}(b-1)}{\sqrt{2\pi}\sigma_X \cdot \left({a_0}^{1-b} - a^{1-b}\right)} \cdot \exp\left\{ -\frac{1}{2}\left[-\frac{\ln\left(\frac{{a_0}^{1-b} - a^{1-b}}{(b-1)}\right) - \ln(tQ)}{\sigma_X} \right]^2 \right\} \end{aligned} \tag{33}$$

Similarly, when $b = 1$, Eqs (31) and (33) can be written as:

$$X = \frac{\ln(a/a_0)}{tQ} \tag{34}$$

$$f_a(a|a_0, t) = \frac{1}{\sqrt{2\pi}\sigma_X a \ln(a/a_0)} \cdot \exp\left\{ -\frac{1}{2}\left[-\frac{\ln(\ln(a/a_0)) - \ln(tQ)}{\sigma_X} \right]^2 \right\} \tag{35}$$

From the above equations, it can be seen that when the initial crack length a_0 (or EIFS) and life t (or critical crack length a_c) are given, the crack length follows a lognormal distribution with mean and variance value are $\ln(tQ)$ and σ_X, respectively. Since the crack length a is a random variable, the full probability formula is used to rewrite Eq. (35) as:

$$f_a(a|t) = \int f_a(a|a_0, t) \cdot f_{a_0}(a_0) \mathrm{d}a_0 \tag{36}$$

2.3.2 EIFS maximum likelihood updating. In order to further improve the accuracy of EIFS and apply its inferred fatigue life in engineering, the update process of the original EIFS distribution form is shown in Figure 3. According to the joint optimization criteria of TTCID and EIFSD, fitting can obtain parameters (α,Q,β,ε, a_r and x_u). The above solving process provides a general solution. However, relevant studies have shown that the obtained 'general solution' is still closely related to the experimental conditions (Shahani and Kashani, 2013; Moreira *et al.*, 2005). Taking the obtained EIFS distribution as an important reference, assuming that the actual EIFS distribution is unknown and there is a prior distribution (TTCI

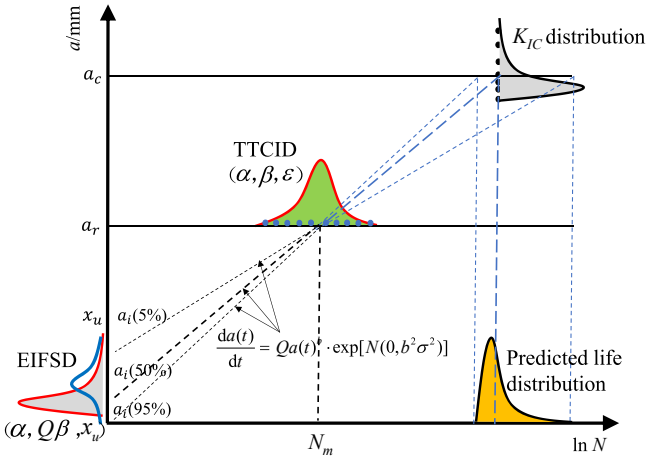

Source(s): Authors own work

Figure 3.
EIFS distribution renewal scheme and life prediction

general solution), the optimized TTCI distribution is further interpolated to obtain the N_i and life median N_m data under optimal a_r. The random crack growth rates under different survival rates were considered N_m, and the EIFS scatter and distribution were derived by inverse derivation according to Eq. (36).

Let the EIFS variable be $v_1, v_2, \ldots, v_n$, and the sample values in the experiment are independent of each other and follow the lognormal distribution, so all likelihood functions also meet the lognormal distribution. There are two factors in this process: 1) the sample set V and the lifetime N_i satisfy the lognormal distribution; 2) consider data acquisition error factors E. In theory, given the number of cycles and the corresponding crack length, lognormal approximation fitting is used to get Eq. (37).

$$f(N_i|V, a_c, E) = \frac{1}{\sqrt{2\pi}N_i\sigma_N}\exp\left\{-\frac{[\lg(N_i) - \lg(F(v, a_c))]^2}{2{\sigma_N}^2}\right\} \tag{37}$$

Among the research methods of EIFS obtained by many scholars, the MLE method is often used to obtain the distribution parameters of the Weibull distribution. Thus, the likelihood function $L(V|D, E)$ of variable V can be obtained as:

$$L(V|D, E) = \prod_{i=1}^{n} f(V|D_i, E) = f(N_i|V, a_c, E) \tag{38}$$

In Eqs (37)-(38), $D_i = (a_i, N_i)$ is the dataset between the number of cycles observed through experiments and the crack length, $F(v, a_c)$ is the crack propagation formula obtained by fitting the known data sample points, with the upper and lower limits of integration being a_c and v_i. The variance σ_N of life N can be obtained through Monte Carlo simulation or directly fitted from the sample life values.

In the process of experiment, real-time monitoring of crack length is obtained, and then the lognormal distribution of parameter X is obtained according to the above function formula. The estimation of its lifetime N was as follows:

$$N = \int_{v_i}^{a_c} \frac{1}{\mathrm{d}a/\mathrm{d}N}\mathrm{d}N = \int_{v_i}^{a_c} \frac{1}{\langle \mathrm{d}a/\mathrm{d}N\rangle \exp(\pm E)}\mathrm{d}N = \langle N\rangle + \exp(\mp E) \tag{39}$$

Assuming the mean and variance of variables EIFS for μ and σ^2, respectively, then,

$$L(\mu, \sigma^2 | D, E) = \prod_{i=1}^{\exists} \int L\left(\widetilde{V}\middle| D, E\right) f\left(\widetilde{V}\middle| E\right) \mathrm{d}\widetilde{V} \tag{40}$$

where $\exists$ is the total number of specimens and $\widetilde{V}$ is the EIFS obtained with errors.

The measurement error caused by temperature change is denoted as ω, the measured experimental data (including the real results of various error effects) are introduced with the noise value of 0.1, and the sample value of the updated variable V is obtained by selecting the optimal TTCID parameters (α, β, ε) and the median life N_{m} corresponding to the reference crack length a, combined with the probability reliability formula. And then μ and σ^2 distributions are calculated:

$$\begin{cases} L(\mu, \sigma^2 | D, w, Cov) = \prod_{i=1}^{\exists} f(\mu, \sigma^2, \mu_V) \\ f(\mu | D, w, Cov) = \dfrac{\int L(\mu, \sigma^2 | D, w, Cov)\mathrm{d}\sigma}{\iint L(\mu, \sigma^2 | D, w, Cov)\mathrm{d}\sigma\mathrm{d}\mu} \\ f(\sigma | D, w, Cov) = \dfrac{\int L(\mu, \sigma^2 | D, w, Cov)\mathrm{d}\mu}{\iint L(\mu, \sigma^2 | D, w, Cov)\mathrm{d}\mu\mathrm{d}\sigma} \end{cases} \tag{41}$$

$$\overline{m}_{EIFS} = \int v g(\mu, \sigma^2, v)\mathrm{d}v \tag{42}$$

Among them, $g(\mu, \sigma^2, v)$ and $\overline{m}_{EIFS}$ are the probability density and mean of the lognormal distribution of EIFS, respectively.

2.3.3 Critical crack length distribution. According to linear elastic fracture mechanics, the maximum stress intensity factor $K_{\max}$ of the crack tip can be expressed as a function between the maximum stress $\sigma_{\max}$ and the crack length $y(a)$:

$$K_{\max} = \sigma_{\max} \cdot y(a) \Rightarrow a = g(K_{\max})/\sigma_{\max} \tag{43}$$

$$f_K(K) = f_a(a) \cdot a' = f_a[g(K_{\max})/\sigma_{\max}]g'(K_{\max})/\sigma_{\max} \tag{44}$$

Considering the geometric correction parameters of a finite plate, the crack length can be expressed as:

$$a = \frac{1}{\pi}\left(\frac{K_{\max}}{YS_{\max}}\right)^2 \tag{45}$$

From Eqs (44)-(45), it can be seen that when fracture toughness K_{Ic} satisfies the lognormal distribution, the limit crack length a_c also satisfies the lognormal distribution. Suppose that the corresponding safety reliability of the structure after reaching the critical crack size is p, that is, $P(K_{Ic} > K_{Ic,p}) = p$, when the confidence is γ, there is

$$\lg K_{Ic,p} = \lg \overline{K}_{Ic} + \mu_p \cdot s_1 \Rightarrow K_{Ic,p,\gamma} = 10^{\lg \overline{K}_{Ic} + \mu_{p,\gamma} \cdot s_1} \tag{46}$$

where $\overline{K}_{Ic}$ is related to the sample number m, and $\mu_{p,\gamma}$ is the p component point on the confidence level, which can be obtained by checking the statistical quantile table. Other parameter values can be obtained by the following formula:

$$\begin{cases} \lg \overline{K}_{Ic} = \dfrac{1}{m} \sum_{i=1}^{m} \lg K_{Ic,i} \\ s_1 = \sqrt{\dfrac{1}{m-1} \sum_{i=1}^{m} \left(\lg K_{Ic,i} - \lg \overline{K}_{Ic} \right)^2} \end{cases} \tag{47}$$

From a statistical perspective, the unbiased estimation of the $K_{Ic,i}$ variable in the normal distribution can be tested using t-distribution, and then the upper integral limit a_c and average $\overline{a}_c$ are obtained according to the random crack growth rate.

The above derivation process is sorted into a flowchart, as shown in Figure 4.

3. Materials and experiment

Since turbine blades often work at different temperatures, the SX material was used in this test, and its elastic properties at different temperatures are shown in Appendix. ASTM E647-15 (ASTM, 2015) mainly recommends three types of specimens, namely, compact tension [C(T)] specimens, middle tension [M(T)] specimens and eccentrically-loaded single edge tension [ESE(T)] specimens for crack growth studies of materials. ESE(T) samples were used in this study, which has the main advantage of providing additional workspace while reducing the amount of processed material. The design reduces the T-stress (the stress parallel to the crack surface) that affects the crack propagation angle, making the crack fracture path more self-similar than other specimens. The size of the specimen is

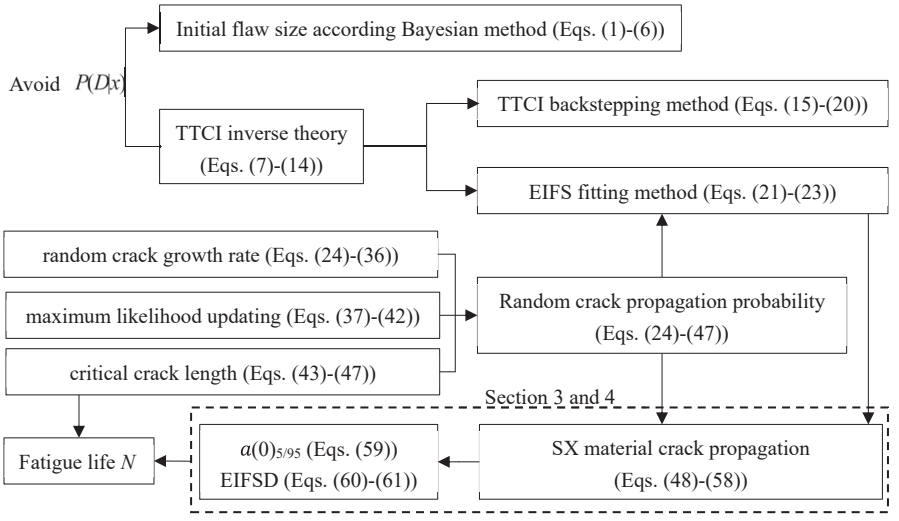

Source(s): Authors own work

Figure 4.
The flowchart for the equations

92.5 × 25 × 2 mm, and the geometric length (tensile) direction is cut along the single crystal blank [001] orientation. A small notch was created on the ESE(T) specimens to induce crack initiation, and the notch was made by EDM. The length and width of the notch were 7.5 and 1.5 mm respectively, and the sharp angle is 30°. Prior to the experiment, the machining caused obvious residual stress and rough surface on the surface of the specimens, which had a large impact on the crack propagation behavior. Therefore, this experimental piece was ground with low stress and matched with manual polishing. The tensile strength, yield strength, elongation of the material, as well as the geometry and physical objects of the ESE(T) specimen are shown in Figure 5.

It can be seen from Figure 5(a) that the tensile properties of the material vary greatly at different temperatures (Committee for Compilation of Materials, 2010). In order to explore the applicability of the EIFS theory of SX materials at different temperatures, and minimize the influence caused by the difference in mechanical properties of materials, while taking into account the accuracy of crack observation and test efficiency, crack propagation tests were carried out at three low-medium temperatures. The maximum test stress σ_{max} remains unchanged at 50 MPa (approximately 5% of the tensile strength), with a stress ratio of 5 Hz and a sine wave load. The test matrix is shown in Table 1.

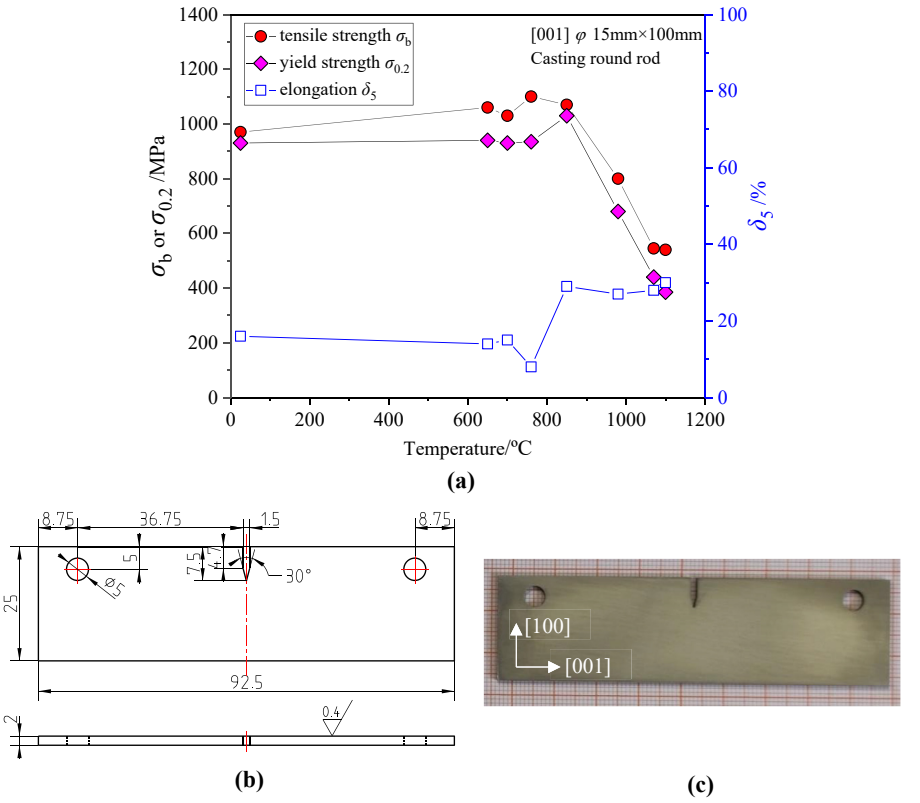

Figure 5.
(a) Mechanical properties of materials and (b)–(c) Specimen drawings and objects (unit: mm)

Source(s): Authors own work

4. Results and discussion

4.1 Crack propagation path and effective driving force

Subcritical crack propagation behavior is studied by using fracture mechanics under different isothermal cyclic loading conditions. Unlike traditional cast polycrystalline materials, the fatigue crack propagation of nickel-based monocrystalline superalloys is along the strong slip band. The crack plane is crystal plane and inclined to the stress axis. Therefore, its cracking patterns are mixed, consisting of modes I, II and III. Typical crystallographic mixed mode cracks at these three different temperatures are shown in Figures 6 and 7 (only several typical fracture modes are shown in the figures). The results indicate that the SX material exhibits fatigue failure at room temperature on the {111} crystal plane, which is inclined to the width and thickness of ESE(T) specimen by about 45°. As the temperature increases, type I cracks perpendicular to the loading axis appear, and the proportion of 650 ℃ exceeds 450 ℃.

Due to the complex geometric shape of cracks, the stress intensity factor solution for type I cracks based on isotropic materials in the ASTM standards does not meet the limited crack inclination angle and material property range. It is clearly necessary to conduct stress intensity factor analysis and calculation for anisotropic SX materials, and provide the stress intensity factor solution for anisotropic ESE (T) specimens with inclined cracks. The expression for the type I stress intensity factor of isotropic ESE(T) specimen provided according to ASTM E647-15 standard (ASTM, 2015):

$$K_{\mathrm{I}} = \frac{L}{BW^{1/2}} F(a/W) \tag{48}$$

Temperature	Maximum stress σ_{max}	Stress ratio	Frequency	Design number	Valid number
25 ℃	50 MPa	0.1	5 Hz	7	6
450 ℃				7	6
650 ℃				7	6

Source(s): Authors own work

Table 1. Test matrix for ESE (T) specimens at different temperatures

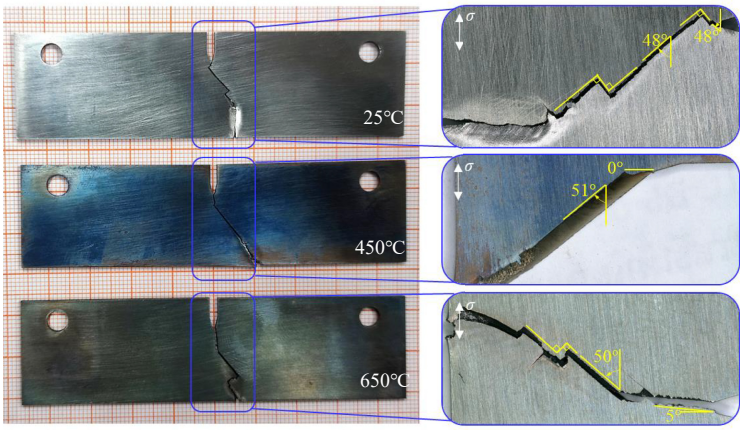

Source(s): Authors own work

Figure 6. Crack propagation forms at different temperatures

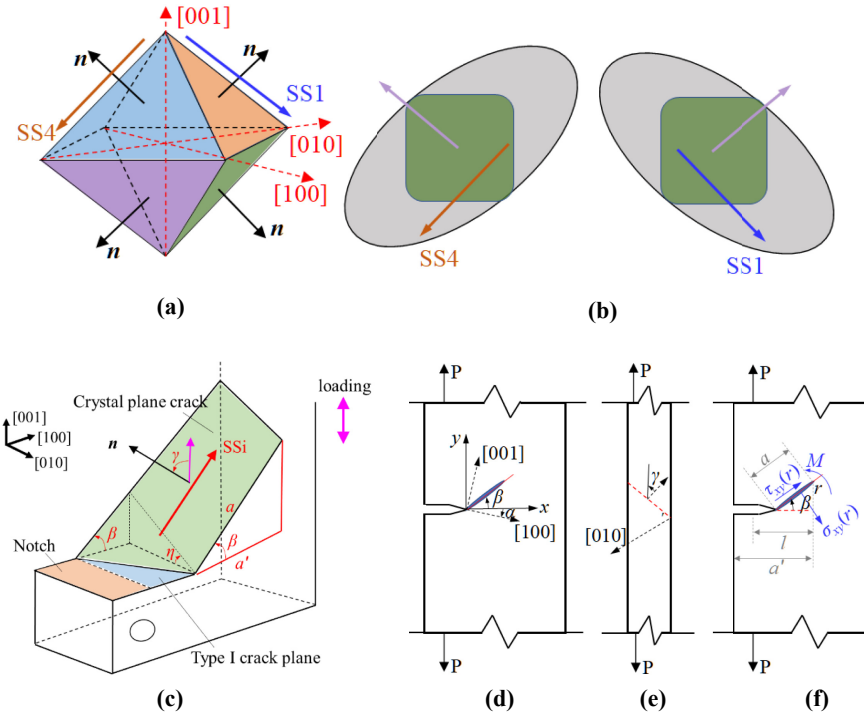

Figure 7.
Fracture schematic diagram of ESE(T) specimen with crack inclination angle: (a) different slip planes and slip directions; (b) two typical slip directions for crack propagation; (c) mixed crack propagation mode; (d) different orientations of material; (e) The inclination angle of the crack along the thickness direction; (f) load and moment balance diagram at crack tip

Source(s): Authors own work

$$F(a/W) = \alpha^{1/2}\frac{1.4+\alpha}{(1-\alpha)^{3/2}}\left(3.97 - 10.88\alpha + 26.25\alpha^2 - 38.9\alpha^3 + 30.15\alpha^4 - 9.27\alpha^5\right) \quad (49)$$

In Eq. (48), L is the applied load (unit: N); α is the ratio of crack propagation length to specimen width, equal to a/W and $0< \alpha <1$. In the study of evaluating the effect of material orthogonality on the SIF solution of ESE(T) specimens through numerical research, Sih *et al.* (1965) used the complex variable method to derive a general equation for the stress field at the crack tip of anisotropic bodies. For cracks in the x_1 direction under plane stress state, Suo *et al.* (1991) and Bao *et al.* (1992) proposed parameter ρ to improve the crack correction coefficient to measure material orthogonality, resulting in an error of less than 1%. To consider the influence of local crystal orientation of the material, the same method was used in Eqs (50)-(52).

$$F_1(a/W) = Y(\rho)F(a/W) \quad (50)$$

$$Y(\rho) = \left[1 + 0.1(\rho-1) - 0.016(\rho-1)^2 + 0.002(\rho-1)^3\right] \Big/ \left[(1+\rho)/2\right]^{1/4} \quad (51)$$

$$\rho = \frac{2S_{12} + S_{66}}{2\sqrt{S_{11}S_{22}}} \quad (52)$$

By analyzing the fracture morphology, cracks often exhibit two mutually perpendicular slip systems (such as SS1 and SS4 in Figures 7(a)–(b)). When considering three-

dimensional octahedral crystal oblique cracks and type I cracks comprehensively (Figure 7(c)), based on the analytical SX material stress field expression (Chan *et al.*, 1987) combined with Eq. (52), the K_{I}, K_{II}, K_{III} and effective stress intensity factor ΔK_{eff} can be obtained in Eqs (53)-(54).

$$\begin{cases} K_{\mathrm{I}} = \dfrac{L\cos^2\gamma}{B\sqrt{W}}F_1(a'/W) \\ K_{\mathrm{II}} = \dfrac{L\cos^2\gamma}{B\sqrt{W}}F_2(a'/W) \\ K_{\mathrm{III}} = \dfrac{L\cos\gamma\sin\gamma}{B\sqrt{W}}F_3(a'/W) \\ a' = 7.5 + a\cos\beta \end{cases} \tag{53}$$

$$\Delta K_{\mathrm{eff}} = \left(\Delta K_{\mathrm{I}}^2 + \frac{C_2}{C_1}\Delta K_{\mathrm{II}}^2 + \frac{C_3}{C_1}\Delta K_{\mathrm{III}}^2\right)^{1/2} \tag{54}$$

Among them,

$$\begin{cases} \mathrm{C}_1 = \dfrac{-S_{22}}{2}\mathrm{Im}\left[\dfrac{\mu_1+\mu_2}{\mu_1\mu_2}\right] \\ C_2 = \dfrac{S_{11}}{2}\mathrm{Im}[\mu_1+\mu_2] \\ C_3 = \dfrac{1}{2}\dfrac{S_{44}S_{55}}{\sqrt{S_{44}S_{55}-S_{45}^2}} \end{cases} \tag{55}$$

The μ_1 and μ_2 in above equation satisfy Eq. (56) and S_{ij} is the flexibility matrix parameter. The specific parameters are shown in the Appendix.

$$S_{11}\mu^4 - 2S_{16}\mu^3 + (2S_{12}+S_{66})\mu^2 - 2S_{26}\mu + S_{22} = 0 \tag{56}$$

The expression of the equivalent stress intensity factor shown in Table 2 can be obtained by combining the flexibility matrix parameters with Eqs (53)-(56).

The discussion of crystal orientation and declination in combination Eq. (53) and Appendix can be concluded that the crack inclination angle has little effect on polycrystalline materials within 30°, but the critical point is not given. Furthermore, the two-dimensional moment balance equation for crack tip load is obtained as follows:

Temperature	μ_1 and μ_2	C_2/C_1	C_3/C_1	Function expression of ΔK_{eff}
25 °C	conjugate complex	4.10	1.94	$(\Delta K_I^2 + 4.10\cdot\Delta K_{II}^2 + 1.94\cdot\Delta K_{III}^2)^{1/2}$
450 °C		4.10	2.02	$(\Delta K_I^2 + 4.10\cdot\Delta K_{II}^2 + 2.02\cdot\Delta K_{III}^2)^{1/2}$
650 °C		4.10	2.07	$(\Delta K_I^2 + 4.10\cdot\Delta K_{II}^2 + 2.07\cdot\Delta K_{III}^2)^{1/2}$

Source(s): Authors own work

Table 2. Equivalent stress intensity factors for ESE(T) specimens at different temperatures

$$\begin{cases} P = B\int_0^r (\sigma_{yy}(r)\cos\beta + \tau_{xy}(r)\sin\beta)\mathrm{d}r \\ Pl = B\int_0^r \sigma_{yy}(r) r\mathrm{d}r \end{cases} \tag{57}$$

As the crack length a and inclination angle($\beta > 30°$) becomes larger, $\sigma_{yy}(r)$ in equation (65) it rapidly increases. As the result, it necessary for $\tau_{xy}(r)$ becomes a negative in order to maintain the equation. In this case, the point where the gradient of $\sigma_{yy}(r)$ or $F_1(a'/W)$ undergoes significant changes can be regarded as the critical value for the positive and negative conversion of $\tau_{xy}(r)$. According to Eq. (57), the maximum value of $\tan\beta/\cos\beta$ is obtained at (0.3, 0.217) (Figure 8), the maximum $F_2(a'/W)$ value is 3.24 and the maximum β angle is 32.2°. For SX material, a large number of studies have also shown that the crack propagation direction will reach 45° or even higher (Zhang *et al.*, 2020), which will result in a single direct projection method not being applicable. Therefore, Sakaguchi *et al.* (2012) considered K_{III} as part of the crack propagation driving force, and the actual crack propagation length is expressed as a, thus, K_{III} in Eq (53) can be rewritten as:

$$\begin{cases} K_{\mathrm{III}} = \dfrac{P\cos\gamma\sin\gamma}{b\sqrt{W}}F_3(a'/W) = \dfrac{6Pa}{BW^2}\cos\gamma\sin\gamma\sqrt{\pi a}F_3(a/W) \\ F_3(a/W) = \sqrt{\dfrac{2W}{\pi a}\tan\left(\dfrac{\pi a}{2W}\right)} \end{cases} \tag{58}$$

4.2 Solution of EIFSD

In the solution results, K_{I} is often relatively small compared to either K_I and K_{III}, and its function expression is relatively complex, so it can be ignored. That is, ΔK_{eff} only retains the ΔK_{I} and ΔK_{III} terms, and the expression of ΔK_{eff} in Eq. (54) and Table 2 is changed.

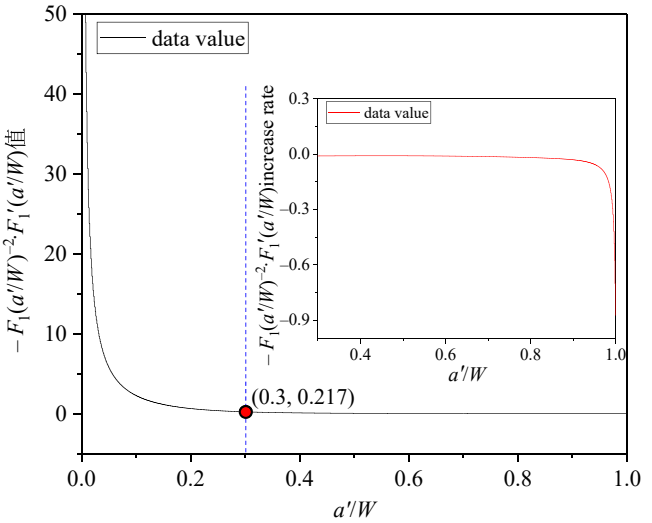

Source(s): Authors own work

Figure 8.
Type I stress intensity factor characterizes the inclined cracks

According to Eq. (25), the $da/dt - a$ and $da/dt - (\Delta K_{eff})$ functions are fitted respectively to verify the goodness of fit and the basic hypothesis of TTCI theory (Figure 9). It should be noted that before the transition from a straight crack to a grain surface crack, it is assumed that $\Delta K_{eff} = \Delta K_I$. Subsequently, the crack propagation data was substituted into the formula

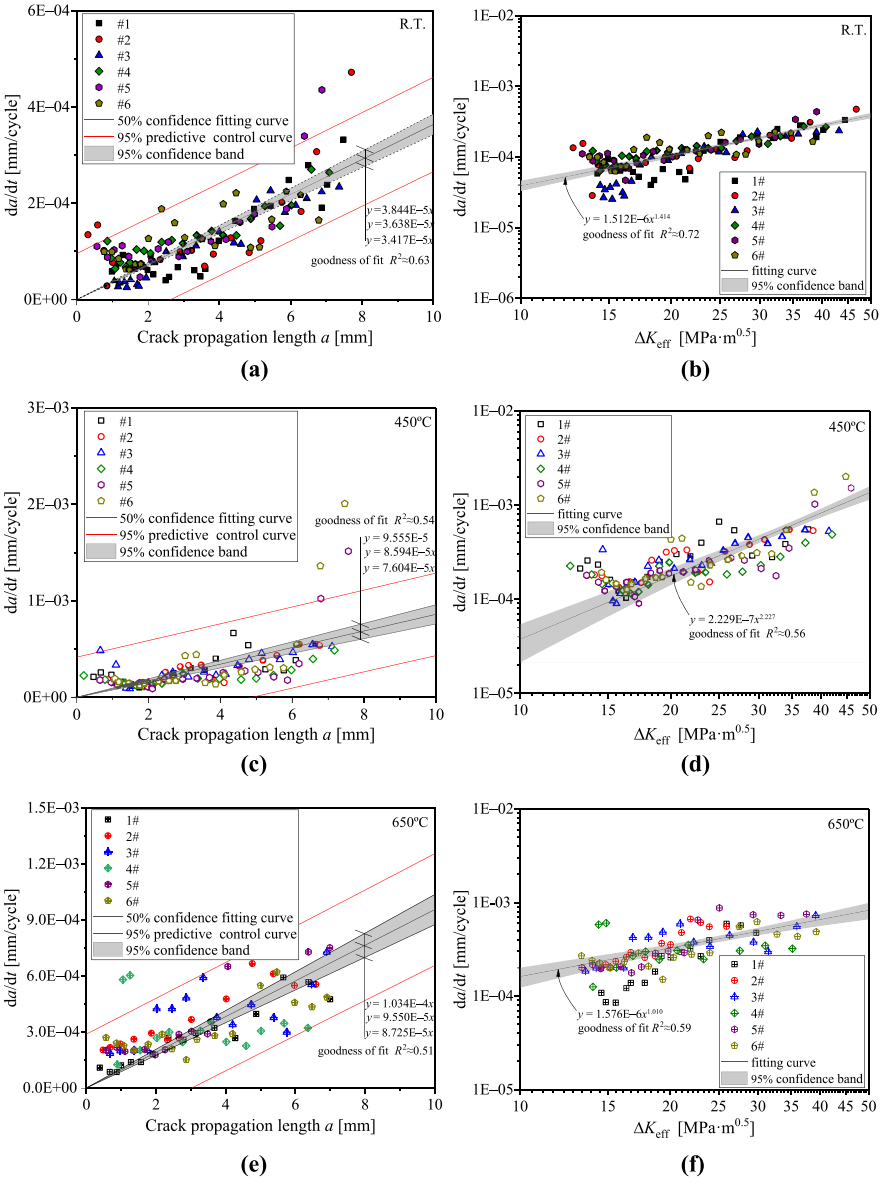

Source(s): Authors own work

Figure 9.
Crack propagation fitting lines at different temperatures: (a)–(b) R.T.; (c)–(d) 450 ℃; (e)–(f) 650 ℃

in Section 2.2, and the iteration sequence was edited based on the MATLAB 2014 platform. The corresponding SSEs for the number of iterations are shown in Figure 10, respectively.

The TTCI backstepping method and EIFS fitting method take the minimum values after 393 iterations and 465 iterations, respectively, and the probability density and distribution function of EIFS can be obtained according to the solving parameters, as shown in Figure 11. It can be concluded from the figure that the average rank distribution can functionalize EIFS and exhibit a probability distribution. Compared to the TTCI backstepping method, the EIFS fitting method yields a data point fitting function that is relatively close to the average rank distribution value, which indirectly indicates that the SEE value in Eqs (20) and (23) is more inclined for the EIFS fitting method. According to the distribution functions, the "double 95" equivalent initial crack size $a(0)_{5/95}$ that meets the 5% failure probability and 95% confidence level requirements can be obtained, which satisfies the formulation:

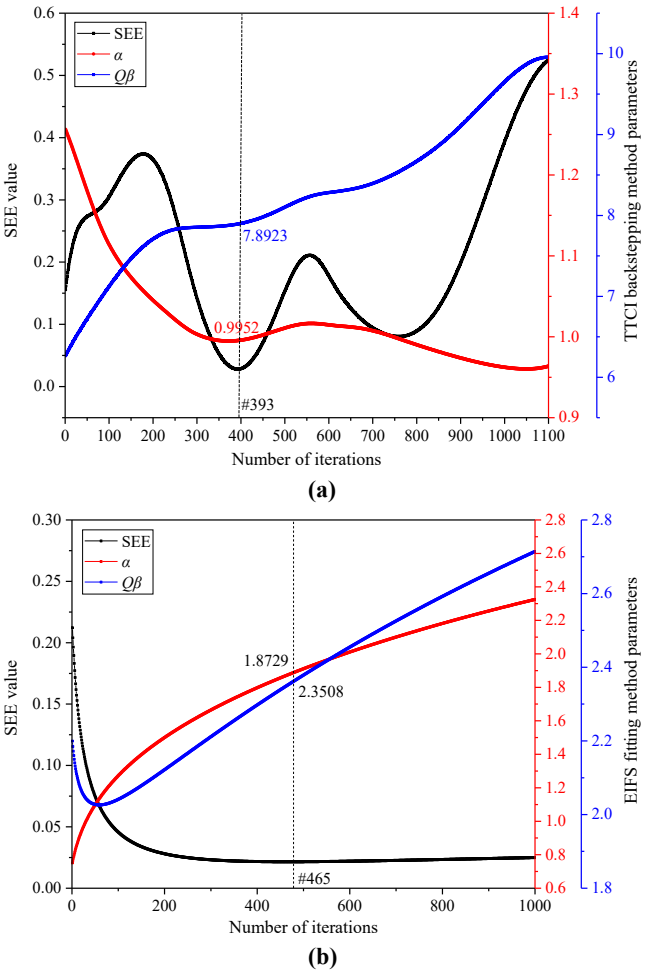

Figure 10.
EIFSD parameter values: (a) TTCI backstepping method and (b) EIFS fitting method

Source(s): Authors own work

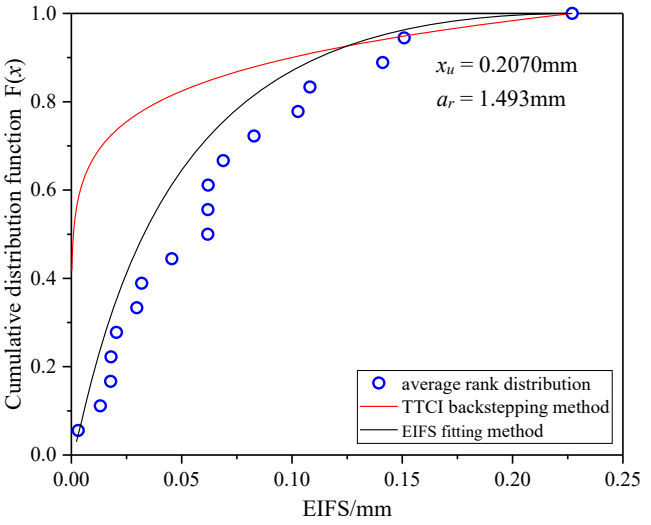

Source(s): Authors own work

Figure 11.
EIFS probability distribution function curve

$$a(0)_{5/95} = x_u \exp\left[-Q\beta(-\ln 0.95)^{1/\alpha}\right] \tag{59}$$

Substitute the parameter values into the above equation, and the calculated values for the TTCI backstepping method and EIFS fitting method are 0.1389 mm and 0.1279 mm, respectively. Similarly, the EIFS values are mainly concentrated within the average rank probability range of 20–80%, with distribution intervals of [0.0072, 0.0399] and [0.0114, 0.0803] (mm), respectively.

By dispersing the EIFSD, the median life (a_r,N_m) can be used as the starting point for the inverse derivation, then the EIFS values at the same temperature can be solved separately. It should be noted that the crack length when the crack extends to the mean life is determined by interpolation. That is, the upper limit of the life integral is derived from the known data combined with the random crack growth rate and predicted life distribution in Section 2.3. Then the lower integral limit is determined according to the average life, that is, the EIFS value. Due to the wider coverage of MLE method scatter, reflecting the actual dispersion, at the same time, the EIFSD solved by EIFS fitting distribution is relatively dense compared with TTCI backstepping method, basically within 0.2 mm. When EIFSD satisfies a lognormal distribution, its probability density is expressed as a function:

$$g(\mu, \sigma^2, v) = \frac{1}{0.8876v\sqrt{2\pi}} \exp\left[-\frac{(\ln v + 2.8683)^2}{1.5757}\right] \tag{60}$$

It can be concluded that the average EIFS value is 0.0842 mm in Eq.(60), and the data are mainly concentrated in the average rank probability of 20%–80%, and the interval of distribution in the data set can be solved as [0.0212, 0.0736] (mm). It should be noted that, when EIFS≈0.25 mm, the distribution function value is close to 1 in the TTCI backstepping method. In other words, the probability expression of the TTCI backstepping method cannot cover the range of EIFS values predicted by the MLE method. In the MLE method, the

calculation interval [0.0316, 0.1128] (mm) contains most of the results of TTCI backstepping calculation. Therefore, an improved TTCI backstepping method is proposed in this paper, which is mainly used to determine the initial EIFS distribution, and the EIFS distribution in the EIFS fitting - MLE method is more suitable, with wider range and higher precision. Similarly, the EIFS values calculated by EIFS fitting method can be fitted and updated with the EIFS distribution of specific specimens. The updated probability density expression is:

$$g_{update}\left(\mu,\sigma^2,v\right)=\frac{1}{0.9164v\sqrt{2\pi}}\exp\left[-\frac{\left(\ln v+3.4039\right)^2}{1.6796}\right] \tag{61}$$

The schematic diagram of its probability density and cumulative distribution function is shown in Figure 12, and $\overline{m}_{EIFS}$ can be calculated as 0.0506 mm. In the figure, it is obvious that the EIFS scatter points distributed according to the average rank with MLE method can be well matched with the fitted probability density.

4.3 Fatigue life prediction

Determine the probability distribution of the critical crack length a_c using the K_{IC} that satisfies the probability distribution (Eq. (47)), and only the average value of the same temperature is considered to simplify the analysis process. According to the test results, the $\overline{a}_c$ values of room temperature, 450 and 650 ℃ can be 7.2112 , 7.1183 and 6.7359 mm respectively. Numerous studies have shown that the upper limit of integration, a_c, has only slight differences in the integration results, especially in the logarithmic normal distribution. Compare the various EIFS evaluation methods mentioned above, select crack propagation functions for different survival rates (5%, 50% and 95%), and predict the total fatigue life and experimental life through Eq. (7) as shown in Figure 13. The upper and lower limits of the error bars correspond to the upper and lower limits of the data survival rate.

It can be clearly seen from the figure that the error between the predicted life of the EIFS fitting method and the test life is very small. The EIFS fitting - MLE method prediction results are better, and the corresponding lives between different temperatures are very close, with the vast majority of results within the double error band range. This is mainly because, on the

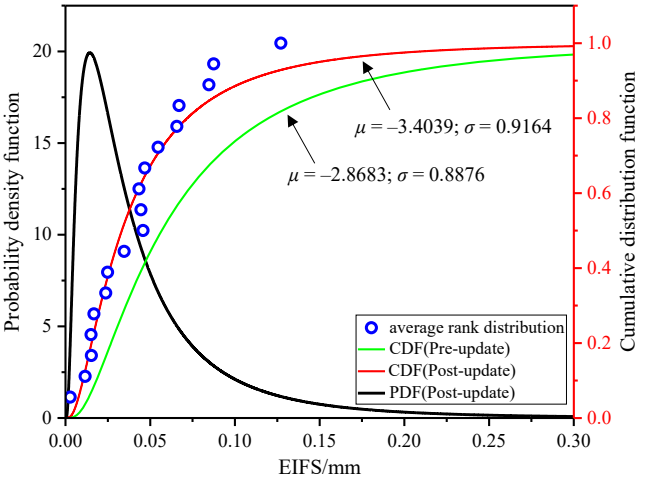

Figure 12.
EIFS probability density and cumulative distribution

Source(s): Authors own work

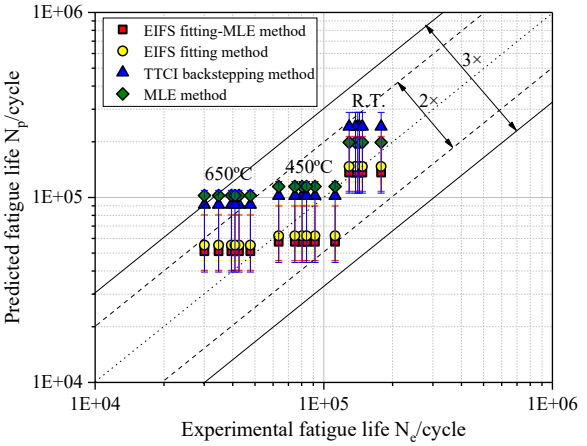

Source(s): Authors own work

Figure 13.
Fatigue life prediction results

one hand, the function expression of crack propagation with high reliability of standard parts is adopted, and repeated experiments are combined to avoid accidental errors and large backstepping errors, resulting in better prediction performance than ordinary test pieces. On the other hand, considering that the EIFS values at different temperatures are the same and meet different guarantee rates, the use of universal EIFS is repeatedly optimized, which can better match the experimental data, and the predicted life of EIFS can be evenly distributed on both sides of the test life.

Undoubtedly, the two methods based on TTCI theory can effectively avoid the problem of EIFS values changing with temperature. It fits the EIFS values obtained under various conditions into a specific Weibull distribution or lognormal distribution. Noted that the fatigue life prediction data not only relies on the average EIFS value, but also satisfies the EIFS survival rate of 5–95% in the data. The TTCI backstepping method error bar is longer than that of the EIFS fitting method. In the prediction results at room temperature, the vast majority results for TTCI backstepping method are within double error band range, but it exceeds double error band at 450 and 650 °C. Although the MLE method has a relatively large deviation compared to other methods in the absence of a prior distribution, most of it is also within a 3-fold error band, but it is clearly temperature related, especially the error between room temperature and high temperature, which is better than TTCI backstepping method at room temperature. Therefore, the advantages of MLE method and EIFS fitting method can better reflect the overall distribution of EIFS, making it more widely applicable.

Fortunately, the range of predicted total fatigue EIFS values based on MLE method and EIFS fitting optimization is approximately [0.0028, 0.0875] (mm), which has little impact on life prediction. Further, although the conventional TTCI backstepping method has a larger error than the optimized EIFS fitting-MLE method, it is better than its simplicity and can still be used in engineering, but the life prediction is generally more aggressive.

5. Conclusion

Based on the background of EIFS quantitative characterization of initial defects, the fatigue life of ESE(T) specimens made of anisotropic SX material at three different temperatures is predicted in this paper. The conclusions are as follows:

(1) TTCI method considering different reference crack lengths and test environments can effectively solve the chronic disease of temperature-related EIFS value. To simplify the analysis process and ensure that b = 1, randomness is imposed on the coefficient Q. According to TTCI backstepping method, the optimal Q, reference crack a_r and approximate EIFS values are obtained, and then the random crack growth coefficient is derived, which is more reasonable than the deterministic crack propagation rate to describe crack behavior.

(2) The crack growth path of SX material at different temperatures presents a mixed form of straight crack and crystal plane crack. Based on the anisotropic correction and the effective driving force ΔK_{eff} coupled by two crack growth modes (K_{I} and K_{III}), the crack growth rate at the near-small crack stage can be effectively described, which verifies the basic hypothesis of TTCI backstepping theory.

(3) The optimized EFSD based on MLE method and EIFS fitting method has the highest accuracy in predicting the total fatigue life, with the range of EIFS values being about [0.0028, 0.0875] (mm), and the mean value of EIFS being 0.0506 mm. The fatigue life calculated by combining the EIFSD with the crack propagation rate under 5–95% survival rates is within a twice dispersion band of the experimental error. The TTCI backstepping method is not excluded in practical engineering application, because it can effectively avoid the problem of large life prediction deviation, and it is more convenient to operate.

(4) The total fatigue life is derived from the effective EIFS values, which are derived from fatigue crack growth data at different temperatures. From this perspective, the results of this paper also provide a reference value for the theory in the quantitative evaluation of the initial fatigue quality of aero engine materials. They are more prone to fatigue cracks when used in high-temperature environments, and the combination of EIFS evaluation at room temperature and fracture mechanics can effectively evaluate the high-temperature fatigue life.

References

Al-Mukhtar, A.M., Biermann, H., Hübner, P. and Henkel, S. (2010), "Determination of some parameters for fatigue life in welded joints using fracture mechanics method", *Journal of Materials Engineering and Performance*, Vol. 19, pp. 1225-1234.

ASTM (2015), *Standard Test Method for Measurement of Fatigue Crack Growth Rates*, ASTM E647-15.

Bao, G., Ho, S., Suo, Z. and Fan, B. (1992), "The role of material orthotropy in fracture specimens for composites", *International Journal of Solids and Structures*, Vol. 29 No. 9, pp. 1105-1116.

Cervellon, A., Cormier, J., Mauget, F. and Hervier, Z. (2017), "VHCF life evolution after microstructure degradation of a Ni-based single crystal superalloy", *International Journal of Fatigue*, Vol. 104, pp. 251-262.

Cervellon, A., Cormier, J., Mauget, F., Hervier, Z. and Nadot, Y. (2018), "Very high cycle fatigue of Ni-based single-crystal superalloys at high temperature", *Metallurgical and Materials Transactions A*, Vol. 49, pp. 3938-3950.

Cervellon, A., Hémery, S., Kürnsteiner, P., Gault, B., Kontis, P. and Cormier, J. (2020), "Crack initiation mechanisms during very high cycle fatigue of Ni-based single crystal superalloys at high temperature", *Acta Materialia*, Vol. 188, pp. 131-144.

Chan, K.S., Hack, J.E. and Leverant, G.R. (1987), "Fatigue crack growth in MAR-M200 single crystals", *Metallurgical and Materials Transactions A*, Vol. 18, pp. 581-591.

Claude, B. and Andre, P. (2013), *Fatigue of Materials and Structures: Application to Damage and design*, John Wiley & Sons, Hoboken.

Committee for Compilation of Materials (2010), "Committee for compilation of materials data handbook for aerospace engine design", in *Materials Data Handbook for Aerospace Engine Design*, 4th ed., Aviation Industry Press.

Correia, JAFO, Blasón, S., De Jesus, A.M.P., Canteli, A.F., Moreira, P.M.G.P. and Tavares, P.J. (2016), "Fatigue life prediction based on an equivalent initial flaw size approach and a new normalized fatigue crack growth model", *Engineering Failure Analysis*, Vol. 69, pp. 15-28.

Gallagher, J.P. and Molent, L. (2015), "The equivalence of EPS and EIFS based on the same crack growth life data", *International Journal of Fatigue*, Vol. 80, pp. 162-170.

Hong, H.U., Kang, J.G., Choi, B.G., Kim, I.S., Yoo, Y.S. and Jo, C.Y. (2011), "A comparative study on thermomechanical and low cycle fatigue failures of a single crystal nickel-based superalloy", *International Journal of Fatigue*, Vol. 33 No. 12, pp. 1592-1599.

Jiang, R., Bull, D.J., Evangelou, A., Harte, A., Pierron, F., Sinclair, I., Preuss, M., Hu, X.T. and Reed, P.A.S. (2018), "Strain accumulation and fatigue crack initiation at pores and carbides in a SX superalloy at room temperature", *International Journal of Fatigue*, Vol. 114, pp. 22-33.

Lamm, M. and Singer, R.F. (2007), "The effect of casting conditions on the high-cycle fatigue properties of the single-crystal nickel-base superalloy PWA 1483", *Metallurgical and Materials Transactions A*, Vol. 38, pp. 1177-1183.

Le Graverend, J.B., Cormier, J., Gallerneau, F., Villechaise, P., Kruch, S. and Mendez, J. (2014), "A microstructure-sensitive constitutive modeling of the inelastic behavior of single crystal nickel-based superalloys at very high temperature", *International Journal of Plasticity*, Vol. 59, pp. 55-83.

Li, F., Wen, Z., Wu, Z., Li, Z., Pei, H., Yin, Q., Mao, Q. and Yue, Z. (2023), "The EIFS-based fatigue life prediction approach of nickel-based single crystals with film cooling holes at elevated temperature", *International Journal of Fatigue*, Vol. 166, 107272.

Liang, J., Wang, Z., Xie, H., Shi, H. and Li, X. (2019), "In situ scanning electron microscopy analysis of effect of temperature on small fatigue crack growth behavior of nickel-based single-crystal superalloy", *International Journal of Fatigue*, Vol. 128, 105195.

Liu, Y. and Mahadevan, S. (2009), "Probabilistic fatigue life prediction using an equivalent initial flaw size distribution", *International Journal of Fatigue*, Vol. 31 No. 3, pp. 476-487.

Liu, C.P., Zhang, X.N., Ge, L., Liu, S.H., Wang, C.Y., Yu, T., Zhang, Y.F. and Zhang, Z. (2017), "Effect of rhenium and ruthenium on the deformation and fracture mechanism in nickel-based model single crystal superalloys during the in-situ tensile at room temperature", *Materials Science and Engineering: A*, Vol. 682, pp. 90-97.

Lu, X., Du, J. and Deng, Q. (2013), "In situ observation of high temperature tensile deformation and low cycle fatigue response in a nickel-base superalloy", *Materials Science and Engineering: A*, Vol. 588, pp. 411-415.

Ma, X., Shi, H., Gu, J., Chen, G., Luesebrink, O. and Hardersd, H. (2010), "In-situ observations of the effects of orientation and carbide on low cycle fatigue crack propagation in a single crystal superalloy", *Procedia Engineering*, Vol. 2 No. 1, pp. 2287-2295.

Makeev, A., Nikishkov, Y. and Armanios, E. (2007), "A concept for quantifying equivalent initial flaw size distribution in fracture mechanics based life prediction models", *International Journal of Fatigue*, Vol. 29 No. 1, pp. 141-145.

Moreira, P.M.G.P., de Matos, P.F.P. and de Castro, P.M.S.T. (2005), "Fatigue striation spacing and equivalent initial flaw size in Al 2024-T3 riveted specimens", *Theoretical and Applied Fracture Mechanics*, Vol. 43 No. 1, pp. 89-99.

Morse, L.A. (2020), *Metamodelling-based Reliability and Life Analysis of Engineering Structures with the Boundary Element method*, Imperial College London, London.

Musinski, W.D. and McDowell, D.L. (2012), "Microstructure-sensitive probabilistic modeling of HCF crack initiation and early crack growth in Ni-base superalloy IN100 notched components", *International Journal of Fatigue*, Vol. 37, pp. 41-53.

Nazé, L., Maurel, V., Eggeler, G., Cormier, J. and Cailletaud, G. (2022), *Nickel Base Single Crystals across Length scales*, Elsevier, London.

Ormastroni, L.M.B., Suave, L.M., Cervellon, A., Villechaise, P. and Cormier, J. (2020), "LCF, HCF and VHCF life sensitivity to solution heat treatment of a third-generation Ni-based single crystal superalloy", *International Journal of Fatigue*, Vol. 130, 105247.

Paris, P. (1963), "A critical analysis of crack propagation laws", *Journal of Basic Engineering*, Vol. 85, pp. 528-533.

Pieracci, A. (1995), "Parameter estimation for Weibull probability distribution function of initial fatigue quality", *AIAA Journal*, Vol. 33 No. 9, pp. 1574-1581.

Reed, R.C. (2008), *The Superalloys: Fundamentals and applications*, Cambridge University Press, Cambridge.

Rémy, L., Geuffrard, M., Alam, A., Köster, A. and Fleury, E. (2013), "Effects of microstructure in high temperature fatigue: lifetime to crack initiation of a single crystal superalloy in high temperature low cycle fatigue", *International Journal of Fatigue*, Vol. 57, pp. 37-49.

Rice, R.C. and Broek, D. (1978), *Evaluation of Equivalent Initial Flaws for Damage Tolerance analysis*, Battelle Columbus Laboratories, Ohio.

Rudd, J. and Gray, T. (1976), "Equivalent initial quality method", *AFFDL-TM-76-83-FBE*.

Sakaguchi, M., Tsuru, T. and Okazaki, M. (2012), "Fatigue crack propagation in thin-wall superalloys component; experimental investigation via miniature CT specimen", *Superalloys*, Vol. 2012, pp. 431-437.

Sakaguchi, M., Komamura, R., Chen, X., Higaki, M. and Inoue, H. (2019), "Crystal plasticity assessment of crystallographic Stage I crack propagation in a Ni-based single crystal superalloy", *International Journal of Fatigue*, Vol. 123, pp. 10-21.

Shahani, A.R. and Kashani, H.M. (2013), "Assessment of equivalent initial flaw size estimation methods in fatigue life prediction using compact tension specimen tests", *Engineering Fracture Mechanics*, Vol. 99, pp. 48-61.

Sih, G.C., Paris, P.C. and Irwin, G.R. (1965), "On cracks in rectilinearly anisotropic bodies", *International Journal of Fracture Mechanics*, Vol. 1, pp. 189-203.

Suo, Z., Bao, G., Fan, B. and Wang, T.C. (1991), "Orthotropy rescaling and implications for fracture in composites", *International Journal of Solids and Structures*, Vol. 28 No. 2, pp. 235-248.

Tan, X.P., Liu, J.L., Jin, T., Hu, Z.Q., Hong, H.U., Choi, B.G., Kim, I.S., Jo, C.Y. and Mangelinck, D. (2013), "Effect of Ru additions on very high temperature creep properties of a single crystal Ni-based superalloy", *Materials Science and Engineering: A*, Vol. 580, pp. 21-35.

Tian, S., Ding, X., Guo, Z., Xie, J., Xue, Y. and Shu, D. (2014), "Damage and fracture mechanism of a nickel-based single crystal superalloy during creep at moderate temperature", *Materials Science and Engineering: A*, Vol. 594, pp. 7-16.

Torregosa, R.F. and Hu, W. (2013), "Probabilistic risk analysis of fracture of aircraft structures using a Bayesian approach to update the distribution of the equivalent initial flaw sizes", *Fatigue and Fracture of Engineering Materials and Structures*, Vol. 36 No. 11, pp. 1092-1101.

Tuegel, E.J., Bell, R.P., Berens, A.P., Brussat, T., Cardinal, J.W., Gallagher, J.P. and Rudd, J. (2018), "Aircraft structural reliability and risk analysis handbook, Volume 1: basic analysis methods", (revised), Structures Technology Branch (AFRL/RQVS), aerospace vehicles division wright-patterson air force base United States.

Wang, D.Y. (1982), "A study of small crack growth under transport spectrum loading", *AGARD Specialist Conference*.

Wang, K.S., Chang, S.T. and Shen, Y.C. (1996), "Dynamic reliability models for fatigue crack growth problem", *Engineering Fracture Mechanics*, Vol. 54 No. 4, pp. 543-556.

Wang, J.P., Liang, J.W., Zhang, D.X., Peng, Y. and Wen, Z. (2023), "The effect of small orientation deviation from [001] to [011] on high-temperature creep properties of nickel-based single crystal", *International Journal of Plasticity*, Vol. 166, 103648.

Yang, J.N., Manning, S.D. (1980), "Distribution of equivalent initial flaw size", San Francisco.

Yi, J.Z., Torbet, C.J., Feng, Q., Pollock, T.M. and Jones, J.W. (2007), "Ultrasonic fatigue of a single crystal Ni-base superalloy at 1000 C", *Materials Science and Engineering: A*, Vol. 443 Nos 1-2, pp. 142-149.

Zhang, L., Zhao, L.G., Roy, A., Silberschmidt, V.V. and McColvin, G. (2019), "In-situ SEM study of slip-controlled short-crack growth in single-crystal nickel superalloy", *Materials Science and Engineering: A*, Vol. 742, pp. 564-572.

Zhang, P., Zhang, L., Baxevanakis, K.P., Zhao, L.G. and Bullough, C. (2020), "Modelling short crack propagation in a single crystal nickel-based superalloy using crystal plasticity and XFEM", *International Journal of Fatigue*, Vol. 136, 105594.

Zhuang, M., Morse, L., Khodaei, Z.S. and Aliabadi, M.H. (2023), "Statistical inference of equivalent initial flaw size distribution for fatigue analysis of an anisotropic material", *Journal of Multiscale Modelling*, Vol. 158.

Appendix

Table A1 shows the elastic constants of SX material at different temperatures.

Temperature/℃	Elasticity modulus/GPa	Poisson's ratio	Shear modulus/GPa
25	131.5	0.344	137.0
700	107.0	0.374	100.2
760	105.5	0.377	105.0
850	98.0	0.383	60.6
980	80.5	0.390	80.4
1070	69.5	0.399	74.2
1100	67.5	0.413	63.8

Source(s): Authors own work

Table A1. Elastic constants

Verify the influence of crack propagation formula under the coupling of crack inclination angle and crystal orientation (Pieracci, 1995), and select two types of crack inclination angles ($\beta = 0$ and 30°) and two crystal orientations ($\alpha = 0$ and 45°) were combined in pairs, and the crack length l was projected in the perpendicular tensile direction of the crack geometry. Within the range of the crack length occupying the total width of the specimen [0.2, 0.8], the isotropic empirical formula for CT specimens in ASTM E466 was used to obtain the conclusion that the quintic function of the empirical formula can be fitted to obtain that different crystal orientation angles have no effect on the propagation behavior of type I cracks (Figure A1). Subsequently, the interference of crystal orientation deflection angle α on type I and II cracks is excluded, and the functional relationship between $f_I(l/W)$ and $f_{II}(l/W)$ with (l/W) are calculated respectively, as shown in Figure A2. When the crack inclination angle changes from 0 to 30°, $f_I(l/W)$ has no effect, but when β reaches 45°, $f_I(l/W)$ will change greatly. For $f_{II}(l/W)$, when the crack inclination α is equal to 30°, $f_{II}(l/W)$ is only about 1/15 of $f_I(l/W)$ under the same (l/W). When β reaches 45°, the initial (l/W) crack length is small ($\leq$0.4), the $f_{II}(l/W)$ is positive and approximately independent of the inclination angle, and then turns negative.

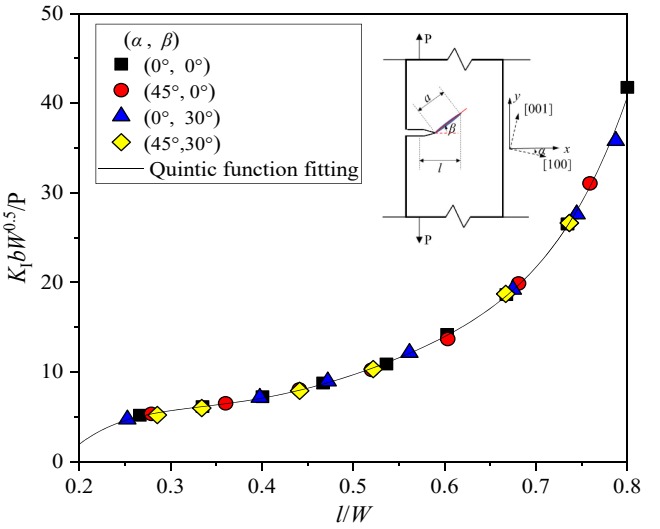

Figure A1.
Influence of different crystal orientation angles on the propagation behavior of type I crack

Source(s): Authors own work

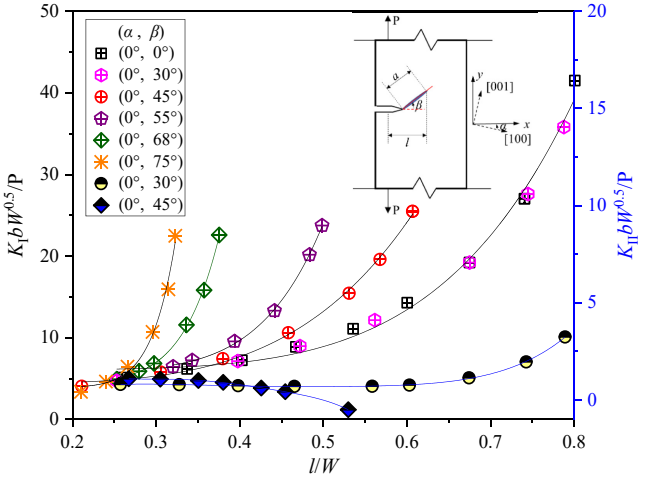

Figure A2.
Effect of different crack inclination on crack propagation behavior of type I and type II

Source(s): Authors own work

Corresponding author
Zhixun Wen can be contacted at: zxwen@nwpu.edu.cn

For instructions on how to order reprints of this article, please visit our website:
www.emeraldgrouppublishing.com/licensing/reprints.htm
Or contact us for further details: **permissions@emeraldinsight.com**